sciendo
ISSN 1335-8871
MEASUREMENT SCIENCE REVIEW
Journal homepage: https://content.sciendo.com

Modeling an Enhanced Modulation Classification Approach using Arithmetic Optimization with Deep Learning for MIMO-OFDM Systems

Venkatramanan M*, Chinnadurai M

E.G.S. Pillay Engineering College, Nagapattinam, Tamilnadu, India. *venkatramanan_m@hotmail.com, mchinnadurai@egspec.org*

Abstract: In a Multiple-Input Multiple-Output Orthogonal Frequency Division Multiplexing (MIMO-OFDM) method, multiple antennas can be used on either the transmitter or receiver end to improve the system capacity, data throughput, and robustness. OFDM has been used as the modulation system that divides the data stream into multiple parallel low-rate subcarriers. MIMO enhances the system by utilizing spatial diversity and multiplexing abilities. Modulation classification in the MIMO-OFDM systems describes the process of recognizing the modulation scheme used by the communicated signals in a MIMO-OFDM communication system. This is a vital step in receiver design as it enables proper demodulation of the received signals. In this paper, an Enhanced Modulation Classification Approach using an Arithmetic Optimization Algorithm with Deep Learning (EMCA-AOADL) is developed for MIMO-OFDM systems. The goal of the presented EMCA-AOADL technique is to detect and classify different types of modulation signals that exist in MIMO-OFDM systems. To accomplish this, the EMCA-AOADL technique performs a feature extraction process based on the Sevcik Fractal Dimension (SFD). For modulation classification, the EMCA-AOADL technique uses a Convolution Neural Network with Long Short-Term Memory (CNN-LSTM) approach. Finally, the hyperparameter values of the CNN-LSTM algorithm can be chosen by using AOA. To highlight the better recognition result of the EMCA-AOADL approach, a comprehensive range of simulations was performed. The simulation values illustrate the better results of the EMCA-AOADL algorithm.

Keywords: Modulation classification, MIMO-OFDM system, deep learning, arithmetic optimization algorithm.

1. INTRODUCTION

Wireless communication is considered an extremely important and major development in today's world. Wireless communication systems require enormously higher data rates and greater transmission reliability to meet the rapidly increasing demands for multimedia applications such as high-quality video and audio [1]. In communication systems, novel wireless applications depend on Multiple Input Multiple Output (MIMO) technology [2]. MIMO can improve data capacity through spatial multiplexing, i.e., data transmission in parallel streams [3]. Orthogonal Frequency Division Multiplexing (OFDM) is a multi-carrier transmission method in which the frequency band can be divided into different orthogonal sub-bands, making the symbol transmitted in each sub-band subject to non-selective frequency fading [4]. The channel equalization is then decreased to a one-tap filter per data symbol. The integration of MIMO transmission and OFDM data modulation is the key requirement for Fourth-Generation (4G) wireless technology.

Automatic Modulation Recognition (AMR) is an intermediate stage between signal demodulation and recognition [5]. This approach can detect the kind of signal modulation and thus acquire the data included in the signals without knowledge of the system parameters. It has been shown that the AMR technique requires the demodulation of signals at the receiver end and is also an important link in wireless communication, which plays a crucial role in both military and civilian domains [6]. In the military sector, AMR technology is used to detect interfering data and important military data [7]. In the civilian sector, AMR is primarily used to monitor the spectrum and detect interference. AMR technology can detect the modulation technique of interfering signals and authorized user signals, study the characteristics of signals, and perform spectrum monitoring. In the following years, with the emergence of AMR technology, the conventional identification techniques can be roughly divided into 2 types, namely, likelihood-based techniques and feature-based techniques [8]. Likelihood-based techniques are theoretically optimal, but the number of computations can be enormous, while feature-based techniques need manual feature extraction, leading to recognition results that are highly dependent on the knowledge of the experts in feature extraction [9]. Therefore, these two identification approaches

DOI: 10.2478/msr-2024-0007
*Corresponding author: venkatramanan_m@hotmail.com (M. Venkatramanan)

are no longer suitable for difficult communication systems. Recently, researchers in the communication domain use standard networks in Deep Learning (DL) systems, which include Convolution Neural Network (CNN) and Recurrent Neural Network (RNN). AMR is a DL-based modulation detection technique that achieved better results than conventional modulation recognition approaches [10].

2. Related works

In [11], the ahors developed a User Terminal (UT) fingerprint placing for multi-cellular large Multiple-Input Multiple-Output Orthogonal Frequency Division Multiplexing (MIMO-OFDM) approach under non-line-of-sight conditions. First, the Deep Neural Network (DNN) presented a novel network framework for the fingerprint localization problem, where the transformer is only based on the self-attention mechanism to directly sequence the fingerprint areas. In [12], a new Fully Connected-DNN (FC-DNN)-based MIMO-OFDM Index Modulation (MIMO-OFDM-IM) for collective identification of transferred symbols from each antenna has been developed and its efficiency can be analyzed. Kalpana and Kesavamurthy [13] proposed a channel estimator based on CNN-Auto Encoder (CNNAE) for MIMO-OFDM techniques. CNNAE is one of the DL methods that provide video signals as input by allocating important learned biases and weights in different targets or features for video signals and are able to distinguish them from each other. Ge et al. [14] have suggested an improved channel equalization system based on DNN. With the aim of shortening the convergence period and improving the learning ability of DNNs, a classifier of weight technique has also been developed to increase the cost function of the DNN, which can be called Classification Weighted-DNN (CW-DNN).

Liu and Lu [15] presented a DL to design a non-iterative detector, according to the structural sparsity of communicated signals in the IM-assisted MIMO-OFDM (IM-MIMO-OFDM) method. First, the authors developed the identification method as a sparse reconstruction issue. Second, a DL-based detector called IMNet was developed to integrate 2 sub-sets with the standard least square algorithm to retrieve the transmitted signal. The authors [16] presented a fingerprint-based position for large MIMO-OFDM technique using Deep CNN (DCNN). By utilizing most benefits of high resolution in the delay and angle domain in a large MIMO-OFDM approach, the authors first proposed an effective Angle-Delay Channel Amplitude Matrix (ADCAM) fingerprint. Then, a DCNN-assisted localization technique was developed to address the modeling error in the fingerprint similarity calculation.

In [17], the authors investigate and compare different effective pilot-based channel estimation systems using NN technology for OFDM technique. The authors introduced other applications of DNN for channel estimation in the investigated OFDM techniques. Chowdary and Rao [18] proposed the Hybrid Mixture Model (HMM) for detecting the spectrum in MIMO method and the efficiency is measured depending on the estimation parameters such as false alarm possibility and identification possibility. The signal obtained through the OFDM antenna was used to analyze the spectral accessibility, where the Eigen statistics and energy of the signal can be generated, which form the input to the HMM. This HMM is a combination of Whale Elephant-Herd Optimizer (WEHO) and Gaussian Mixture Model (GMM).

3. The proposed model

In this manuscript, we have designed and developed an automated modulation recognition technique called Enhanced Modulation Classification Approach using an Arithmetic Optimization Algorithm with Deep Learning (EMCA-AOADL) for MIMO-OFDM systems. The primary goal of the presented EMCA-AOADL technique is to detect and classify different types of modulation signals that occur in MIMO-OFDM systems. To achieve this, the EMCA-AOADL technique follows an Sevcik Fractal Dimension (SFD)-based feature extractor, CNN with Long Short-Term Memory (CNN-LSTM)-based modulation classification, and an AOA-based parameter tuning. Fig. 1 describes the entire procedure of the EMCA-AOADL method.

A. Feature extractor

The SFD algorithm is used to derive a feature vector. During this phase, the fractal feature in the communication signals can be removed using the SFD system [19]. With the self-similar size, it is difficult to utilize objects that might not be self-similar, and box size is used to overcome this problem. During the metric space (X, d), A moves towards M non-empty emergency cluster of X. Box with side length of ε, the lesser values $N(A, \varepsilon)$ of the box required for covering A are formulated as:

$$N(A, \varepsilon) = \{M: A \subset \sum_{i=1}^{M} N(x_i, \varepsilon)\}, \quad (1)$$

where $x_1, x_2, \cdots x_M$ denote the dissimilar points of X. Where ε potential 0, the box size is expressed in (2):

$$D_b = \lim_{\varepsilon \to 0} \frac{InN(A,\varepsilon)}{In(1/\varepsilon)} \quad (2)$$

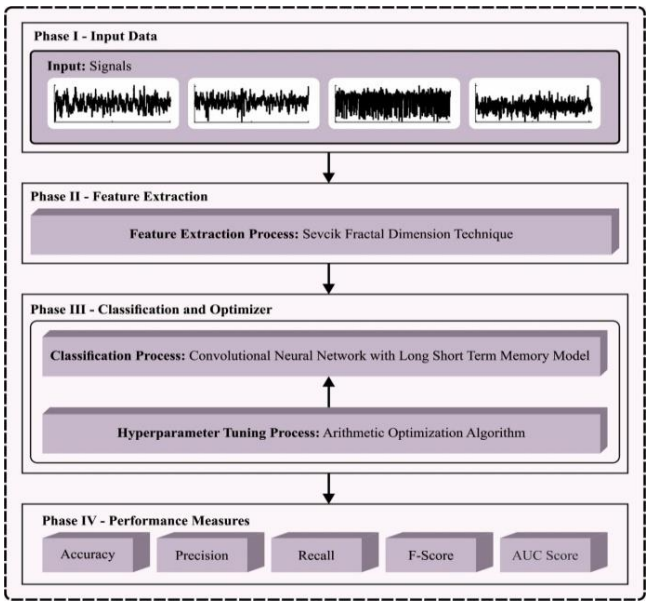

Fig. 1. Workflow of the EMCA-AOADL technique.

As mentioned above, let the signal comprise sequences of points (x_i, y_i), and the signal length be N. Primarily, the signal is standardized:

$$x_i^* = \frac{x_i - x_{\min}}{x_{\max} - x_{\min}}, y_i^* = \frac{y_i - \min}{y_{\max} - y_{\min}} \quad (3)$$

x_{min}, y_{min} represent the minimum values among x_j, y_j. $x_{\max}, y_{\max}$ represent the maximum values among x_j, y_j. Then, the Sevcik fractal dimensional D is measured as follows:

$$D = 1 + \frac{ln(L) + ln(2)}{ln[2 \times (N-1)]} \quad (4)$$

where L represents the length of the waveform as:

$$L = \sum_{i=0}^{N-2} \sqrt{(y_{i+1}^* - y_i^*)^2 + (x_{i+1}^* - x_i^*)^2} \quad (5)$$

B. Modulation recognition using CNN-LSTM method

In this work, the CNN-LSTM approach can be used for the recognition of different types of modulation signals. CNN is a kind of DL model with exceptional capabilities in the field of pattern detection [20]. The main structural layer assumes a filter or kernel which it runs over the data and generates a mapping feature.

$$(f * g)_{(c_1, c_2)} = \sum_{c_1, c_2} f(a_1, a_2) \cdot g(b_1, b_2) \quad (6)$$

In (6), f represents the data and g represents the kernel, $a_1 + b_1 = c_1$ and $a_2 + b_2 = c_2$. Due to the complicated convolutional functions, the pooling and convolution layers are used to simplify the collected features. Typically, the FC layer is used at the architecture end, which is responsible for the classification into corresponding groups.

CNN-LSTM is a hybrid DL mechanism that attempts to synthesize the capabilities of the convolution network and the LSTM. The feature extracted by the CNN is passed to the LSTM, a structure of the RNN, to capture the temporal dependency. Fig. 2 shows the infrastructure of the CNN-LSTM.

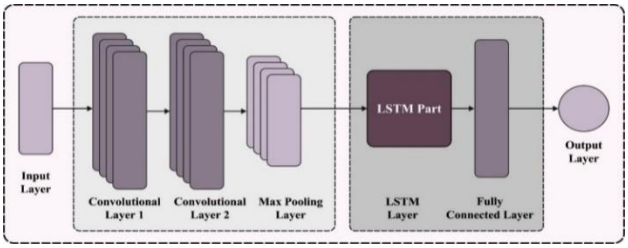

Fig. 2. CNN-LSTM architecture.

The memory cell C_z is the critical re-modelling in RNN:

$$f_z = \sigma\left(W_f \cdot [h_{z-1}, x_z] + b_f\right) \quad (7)$$

$$i_z = \sigma(W_i \cdot [h_{z-1}, x_z] + b_i) \quad (8)$$

$$C_z emp = tanh(W_C \cdot [h_{z-1}, x_z] + b_C) \quad (9)$$

$$c_z = f_z * c_{z-1} + i_z * c_z emp \quad (10)$$

$$O_z = \sigma(W_o \cdot [h_{z-1}, x_z] + b_o) \quad (11)$$

$$h\_z = o\_z * tanh(C\_z) \quad (12)$$

Here C, i, O, and f represent the cell activation vector, the input gate, the output gate, and the forget gate, which have a similar size to the h hidden state. W denotes the weight matrix. W_C stands for the weight of activation cells.

To achieve focal loss for compensating the difficulties of typical cross-entropy loss due to data imbalance problems, a modulating feature was multiplied by the cross-entropy loss.

$$FL(p_z) = -(1 - p_z)^{\gamma} log(p_z) \quad (13)$$

where $\gamma \geq 0$ refers to a tunable focusing parameter.

C. Parameter tuning using AOA

Finally, the hyperparameter values of the CNN-LSTM approach are chosen by using AOA. AOA starts with the population (partially or fully immersed object) [21]. Each object assumes an arbitrary acceleration, density, and volume. Consequently, all objects have an arbitrary location in the fluid. The fitness of each population is evaluated at each iteration until telling maximum iteration or ending criteria are reached. The AOA improves the required main function depending on dissimilar steps. The procedure for using AOA to optimize the stability of the system.

The steps of AOA are described below:

Initialization:

First, each object (population) is randomly positioned based on (14). Next, the volume and density of the objects are randomly initialized based on (15) and (16). Consequently, the acceleration of the object is randomly initialized based on (17).

$$O_i = lb_i + rand \times (ub_i - lb_i), \; i = 1,2,\cdots,N \quad (14)$$

$$\rho_i = rand(0,1) \quad (15)$$

$$V_i = rand(0,1) \quad (16)$$

$$a_i = lb_i + rand \times (ub_i - lb_i) \quad (17)$$

The upper and lower limitations of the i^{th} object are represented accordingly as ub_i and lb_i. O_i denotes the location of the i^{th} object with the maximum size N. The density, volume, and acceleration of the object are formulated accordingly with p, V, and a. The volume and density are randomly distributed in zero and one.

D. Updating density and volume

The densities and volumes of objects can be adjusted using the following expression:

$$\rho_i^{t+1} = \rho_i^t + rand \times (\rho_{best} - \rho_i^t) \quad (18)$$

$$y_i^{t+1} = y_i^t + rand \times (y_{best} - y_i^t) \quad (19)$$

where the volume and density of the better objects are formulated accordingly as y_{best} and ρ_{best}.

E. Transfer operator and density factor

The object was exposed to the collision, then all objects change their location to reach a state of equilibrium. The T_f transfer operator changes the operation stage based on (20). The exploration stage (global) is converted to the exploitation stage (local).

$$T_f = exp\left(\frac{t-t_{max}}{t_{max}}\right) \tag{20}$$

The density factor d, which decreases, helps AOA to reach the near-global performance as follows:

$$d^{t+1} = exp\left(\frac{t_{max}-t}{t_{max}}\right) - \left(\frac{t}{t_{max}}\right) \tag{21}$$

In (20) T_f, varies gradually between 0.0 and 1.0. d factor decreases gradually with time. $t_{\max}$ shows the maximum iteration count.

The collision of objects occurs when $T_f \leq 0.5$. Consequently, the acceleration of the object can be upgraded for $t+1$ iterations according to random material acceleration as

$$a_i^{t+1} = \frac{\rho_{mr}+V_{mr}\times acc_{mr}}{\rho_i^{t+1}\times V_i^{t+1}} \tag{22}$$

In (22), the exploration and exploitation changes based on the transfer operator. If $T_f \leq 0.5$, the exploration occurs in 1/3 of the iterations.

F. Exploration stage (collision between objects)

Furthermore, there is no collision if $T_f > 0.5$. For $f+1$ iterations, the acceleration is estimated using the following equation.

$$a_{\mathrm{i}}^{t+1} = \frac{\rho_{best}+V_{best}\times a_{best}}{\rho_i^{t+1}\times V_i^{t+1}} \tag{23}$$

In (23), a_{best} refers to the acceleration of the better object.

G. Normalize acceleration

Here, the acceleration of the i^{th} object was normalized for the calculation of the percentage of change.

$$a_{i-norm}^{t+1} = u \times \frac{a_i^{t+1}-min(a)}{max(a)-min(a)} + l \tag{24}$$

In (24), the normalization range is within (0.1−0.9). The lower and upper boundaries are represented as l and u accordingly. Reducing the acceleration factors helps to move from local to global solutions.

H. Update position

If $T_f \leq 0.5$ (exploration stage), update the location of the i^{th} object for the latest $t+1$ iteration according to (25). Or, if $T_f > 0.5$ (exploitation stage), update the location according to (26).

$$x_i^{t+1} = x_i^t + K_1 \times rand \times a_{i-norm}^{t+1} \times d \times (x_{rand} - x_i^t) \tag{25}$$

$$x_i^{t+1} = x_{best}^t + F \times K_2 \times rand \times a_{i-norm}^{t+1} \times d \times (T \times x_{best} - x_i^t) \tag{26}$$

$$T = K_3 \times T_f \tag{27}$$

where T differs by the transfer operator and time $[K_3 \times 0.3,1]$ and is estimated by (25). K_1, K_2, and K_3 are constants. T starts with a lower percentage and then gradually increases until it approaches the better location. Consequently, balance the exploitation and exploration stages. The flag F changes the direction of motion based on (28).

$$F = \begin{cases} +1 \; if \; P \leq 0.5 \\ -1 \; if \; P > 0.5 \end{cases}, P = 2 \times rand - K_4 \tag{28}$$

I. Evaluation

Calculate the Fitness Function (FF) for all objects at each iteration and compare the better performance for all iterations and save the achieved better fitness.

The AOA method improves an FF to achieve the best classifier results. It explains a positive integer to indicate the good solution of candidate efficiencies. Here, the reduced error rate of the classifier can be taken as FF as written in (29).

$$fitness(x_i) = ClassifierErrorRate(x_i)$$
$$= \frac{No.of misclassified instances}{Total no.of instances} * 100 \tag{29}$$

4. RESULTS AND DISCUSSION

The modulation recognition results of the EMCA-AOADL method were tested on the modulation signal database, which comprises 1600 instances with 8 classes, as shown in Table 1.

Table 1. Description of the database.

Class	Number of instances
2ASK	200
4ASK	200
2FSK	200
4FSK	200
8FSK	200
BPSK	200
16QAM	200
32QAM	200
Total instances	1600

In Table 2, the comprehensive classification results of the EMCA-AOADL system are examined using 70:30 of the Training (TR) set/ Testing (TS) set. Fig. 3 shows the modulation recognition results of the EMCA-AOADL method at 70% of the TR set. The results illustrate the superior performance of the EMCA-AOADL method. For 2ASK, the EMCA-AOADL method provides $accu_y$, $prec_n$, $reca_l$, F_{score}, and AUC_{score} values of 100%, 100%, 100%, 100%, and 100%, respectively. For 8FSK, the EMCA-AOADL method also provides $accu_y$, $prec_n$, $reca_l$, F_{score},

and AUC_{score} values of 99.82%, 99.24%, 99.24%, 99.24%, and 99.57%, respectively. Finally, for 32QAM, the EMCA-AOADL method provides $accu_y$, $prec_n$, $reca_l$, F_{score}, and AUC_{score} values of 100%, 100%, 100%, 100%, and 100%, respectively.

Table 2. Modulation recognition results of the EMCA-AOADL technique using 70:30 of TR set/TS set.

Class TR set (70%)	$Accu_y$	$Prec_n$	$Reca_l$	F_{score}	AUC_{score}
2ASK	100.00	100.00	100.00	100.00	100.00
4ASK	99.73	99.29	98.59	98.94	99.24
2FSK	99.91	100.00	99.27	99.63	99.64
4FSK	100.00	100.00	100.00	100.00	100.00
8FSK	99.82	99.24	99.24	99.24	99.57
BPSK	99.64	97.24	100.00	98.60	99.80
16QAM	99.82	100.00	98.56	99.28	99.28
32QAM	100.00	100.00	100.00	100.00	100.00
Average	99.87	99.47	99.46	99.46	99.69
Class TS set (30%)	$Accu_y$	$Prec_n$	$Reca_l$	F_{score}	AUC_{score}
2ASK	100.00	100.00	100.00	100.00	100.00
4ASK	99.79	100.00	98.28	99.13	99.14
2FSK	100.00	100.00	100.00	100.00	100.00
4FSK	100.00	100.00	100.00	100.00	100.00
8FSK	100.00	100.00	100.00	100.00	100.00
BPSK	99.79	98.33	100.00	99.16	99.88
16QAM	100.00	100.00	100.00	100.00	100.00
32QAM	100.00	100.00	100.00	100.00	100.00
Average	99.95	99.79	99.78	99.79	99.88

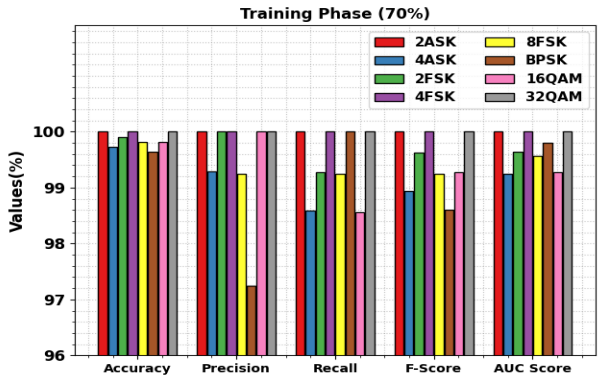

Fig. 3. Modulation recognition results of the EMCA-AOADL method at 70% of the TR set.

Fig. 4 shows the modulation recognition results of the EMCA-AOADL method at 30% of the TS set. The results illustrate the superior performance of the EMCA-AOADL system. For 2ASK, the EMCA-AOADL method provides $accu_y$, $prec_n$, $reca_l$, F_{score}, and AUC_{score} values of 100%, 100%, 100%, 100%, and 100%, respectively. For 2FSK, the EMCA-AOADL method provides $accu_y$, $prec_n$, $reca_l$, F_{score}, and AUC_{score} values of 100%, 100%, 100%, 100%, and 100%, respectively. Also, for 8FSK, the EMCA-AOADL method provides $accu_y$, $prec_n$, $reca_l$, F_{score}, and AUC_{score} values of 100%, 100%, 100%, 100%, and 100%, respectively. Finally, for 32QAM, the EMCA-AOADL method provides $accu_y$, $prec_n$, $reca_l$, F_{score}, and AUC_{score} values of 100%, 100%, 100%, 100%, and 100%, respectively.

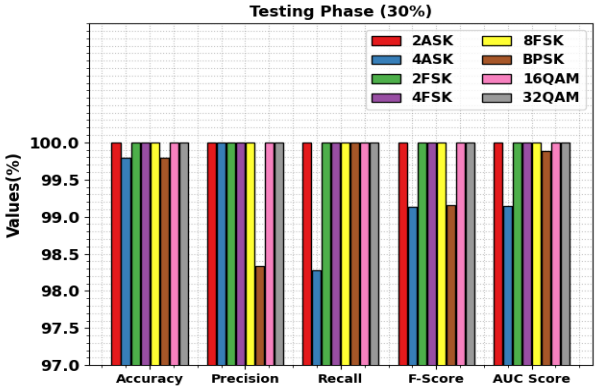

Fig. 4. Modulation recognition results of the EMCA-AOADL method at 30% of the TS set.

Fig. 5 shows an average modulation recognition result of the EMCA-AOADL method. The figure shows that the EMCA-AOADL method has categorized the 8 types of modulation signals. At 70% of the TR set, the EMCA-AOADL method provides $accu_y$, $prec_n$, $reca_l$, F_{score}, and AUC_{score} values of 99.87%, 99.47%, 99.46%, 99.46%, and 99.69%, respectively. At the same time, at 30% of the TS set, the EMCA-AOADL method provides $accu_y$, $prec_n$, $reca_l$, F_{score}, and AUC_{score} values of 99.95%, 99.79%, 99.78%, 99.79%, and 99.88%, respectively.

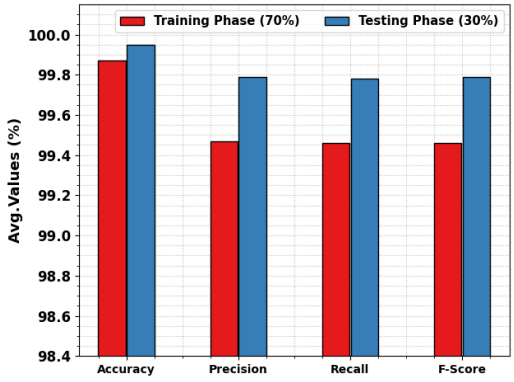

Fig. 5. Average of the EMCA-AOADL method at 70:30 of the TR set/TS set.

Tabl 3. Comparative results of the EMCA-AOADL method with the existing systems.

Algorithm	$Accu_y$	$Prec_n$	$Reca_l$	F_{score}
EMCA-AOADL	99.95	99.79	99.78	99.79
GRA Model	98.12	96.15	98.82	96.43
KNN Model	97.78	96.70	97.63	96.50
BP Model	95.65	94.55	94.48	96.83
RF Model	97.76	97.78	95.35	94.63
BiLSTM-FCN	97.95	97.89	96.65	97.32
COSBO-BiLSTM	97.06	98.63	96.75	98.27

Also based on $prec_n$, the EMCA-AOADL method provides a higher $prec_n$ of 99.79%, while the existing GRA, KNN, BP, RF, BiLSTM-FCN, and COSBO-BiLSTM methods achieved lower $prec_n$ values of 96.15%, 96.70%, 94.55%, 97.78%, 97.89%, and 98.63%, respectively. Based on $reca_l$, the EMCA-AOADL method yields a maximum $reca_l$ of 99.78%, while the existing GRA, KNN, BP, RF, BiLSTM-FCN, and COSBO-BiLSTM methods achieve lower $reca_l$ values of 98.82%, 97.63%, 94.48%, 95.35%, 96.65%, and 96.75%, respectively. These simulation values indicate that the EMCA-AOADL method performs better compared to the other techniques in various measurements.

5. Conclusion

In this manuscript, we have presented an automated modulation recognition technique called EMCA-AOADL for MIMO-OFDM systems. The main objective of the presented EMCA-AOADL algorithm is to detect and classify different types of modulation signals that occur in MIMO-OFDM systems. To achieve this, the EMCA-AOADL technique follows an SFD-based feature extractor, a CNN-LSTM-based modulation classification, and an AOA-based parameter tuning. For modulation classification, the EMCA-AOADL technique has used the CNN-LSTM model. Finally, the hyperparameter values of the CNN-LSTM algorithm are selected using AOA. To emphasize the greater recognition solution of the EMCA-AOADL method, a comprehensive range of simulations can be performed. The simulation values illustrate the promising results of the EMCA-AOADL algorithm.

References

[1] Venkatramanan, M., Chinnadurai, M. (2024). Channel estimation in MIMO TFT-OFDM using hybrid BESOA-CSOA algorithms. *Technical Gazette*, 31 (1), 151-155. https://doi.org/10.17559/TV-20230502000598

[2] He, H., Jin, S., Wen, C.-K., Gao, F., Li, G. Y., Xu, Z. (2019). Model-driven deep learning for physical layer communications. *IEEE Wireless Communications*, 26 (5), 77-83. https://doi.org/10.1109/MWC.2019.1800447

[3] Qin, Z., Ye, H., Li, G. Y., Juang, B.-H. F. (2019). Deep learning in physical layer communications. *IEEE Wireless Communications*, 26 (2), 93-99. https://doi.org/10.1109/MWC.2019.1800601

[4] Al-Rayif, M. I. (2021). PAPR reduction method based on in-phase/quadrature data symbol components in MIMO-OFDM systems. *Journal of Communications Software and Systems*, 17 (4), 326-333. https://doi.org/10.24138/jcomss-2021-0123

[5] Jayamathi, A., Jayasankar, T., Vinoth Kumar, K. (2022). Novel selective mapping with oppositional hosted cuckoo optimization algorithm for PAPR reduction in 5G UFMC systems. *Technical Gazette*, 29 (2), 464-471. https://doi.org/10.17559/TV-20210524085655

[6] Kavitha, G., Deny, J. (2023). Single and multi-point non-orthogonal multiple access based power adaptive design for improving bit error ratio. *Measurement Science Review*, 23 (4), 184-191. https://doi.org/10.2478/msr-2023-0024

[7] Wang, T., Wen, C.-K., Jin, S., Li, G. Y. (2019). Deep learning-based CSI feedback approach for time-varying massive MIMO channels. *IEEE Wireless Communications Letters*, 8 (2), 416-419. https://doi.org/10.1109/LWC.2018.2874264

[8] Vijay Anand, J., Manoharan, P. S., Jeyadheep Vignesh, J., Varatharajan, M., Rubina Sherin, M. (2021). Spider search algorithms for MIMO system and assessment using simatic PCS7. *Technical Gazette*, 28 (4), 1118-1126. https://doi.org/10.17559/TV-20200513113443

[9] Yang, Y., Gao, F., Ma, X., Zhang, S. (2019). Deep learning-based channel estimation for doubly selective fading channels. *IEEE Access*, 7, 36579-89. https://doi.org/10.1109/ACCESS.2019.2901066

[10] Soltani, M., Pourahmadi, V., Mirzaei, A., Sheikhzadeh, H. (2019). Deep learning-based channel estimation. *IEEE Communications Letters*, 23 (4), 652-655. https://doi.org/10.1109/LCOMM.2019.2898944

[11] Han, S., Oh, Y., Song, C. (2019). A deep learning based channel estimation scheme for IEEE 802.11p systems. In *IEEE International Conference on Communications (ICC 2019)*. IEEE. https://doi.org/10.1109/ICC.2019.8761354

[12] Liao, Y., Hua, Y., Dai, X., Yao, H., Yang, X. (2019). ChanEstNet: A deep learning based channel estimation for high-speed scenarios. In *IEEE International Conference on Communications (ICC 2019)*. IEEE. https://doi.org/10.1109/ICC.2019.8761312

[13] Jiang, R., Wang, X., Cao, S., Zhao, J., Li, X. (2019). Deep neural networks for channel estimation in underwater acoustic OFDM systems. *IEEE Access*, 7, 23579-23594. https://doi.org/10.1109/ACCESS.2019.2899990

[14] Alshahrani, E., Alghazzawi, D., Alotaibi, R., Rabie, O. (2022). Adversarial attacks against supervised machine learning based network intrusion detection systems. *PLoS One*, 17 (10), e0275971. https://doi.org/10.1371/journal.pone.0275971

[15] Wang, M., Wang, A., Liu, Z., Chai, J. (2023). Deep learning based channel estimation method for mine OFDM system. *Scientific Reports*, 13 (1), 17105. https://doi.org/10.1038/s41598-023-43971-5

[16] Melacci, S., Ciravegna, G., Sotgiu, A., Demontis, A., Biggio, B., Gori, M., Roli, F. (2022). Domain knowledge alleviates adversarial attacks in multi-label classifiers. *IEEE Transactions on Pattern Analysis and Machine Intelligence*, 44 (12), 9944-9959. https://doi.org/10.1109/TPAMI.2021.3137564

[17] Lal, S., Rehman, S. U., Shah, J. H., Meraj, T., Rauf, H. T., Damaševičius, R., Mohammed, M. A., Abdulkareem, K. H. (2021). Adversarial attack and defence through adversarial training and feature fusion for diabetic retinopathy recognition. *Sensors*, 21 (11), 3922. https://doi.org/10.3390/s21113922

[18] Elnakeeb, A., Mitra, U. (2021). Bilinear channel estimation for MIMO OFDM: Lower bounds and training sequence optimization. *IEEE Transactions on Signal Processing*, 69, 1317-1331. https://doi.org/10.1109/TSP.2021.3056591

[19] Soares, J. A., Mayer, K. S., de Castro, F. C. C., Arantes, D. S. (2021). Complex-valued phase transmittance RBF neural networks for massive MIMO-OFDM receivers. *Sensors*, 21 (24), 8200. https://doi.org/10.3390/s21248200

[20] Ali, K. S., Khan, A. A., T, P., Ur Rehman, A., Ouahada, K. (2023). Learned-SBL-GAMP based hybrid precoders/combiners in millimeter wave massive MIMO systems. *PLoS One*, 18 (9), e0289868 https://doi.org/10.1371/journal.pone.0289868

[21] Naqvi, S. H. R., Ho, P. H., Peng, L. (2021). 5G NR mmWave indoor coverage with massive antenna system. *Journal of Communications and Networks*, 23 (1), 1-11. https://doi.org/10.23919/JCN.2020.000031

Received October 23, 2023
Accepted February 05, 2024